Experimental measurement and modelling of reactive species generation in TiO_2 nanoparticle photocatalysis

Andrea Turolla [a], Andrea Piazzoli [a], Jeffrey Farner Budarz [b], Mark R. Wiesner [b], Manuela Antonelli [a,*]

[a] *Politecnico di Milano, DICA – Environmental Section, Piazza Leonardo da Vinci 32, 20133 Milano, Italy*
[b] *Duke University, Department of Civil and Environmental Engineering, Pratt School of Engineering, 27708 Durham, NC, United States*

Received 4 December 2014
Received in revised form 28 February 2015
Accepted 2 March 2015
Available online 9 March 2015

A B S T R A C T

The generation of reactive species in titanium dioxide (TiO_2) nanoparticle photocatalysis was assessed in a laboratory scale setup, in which P25 Aeroxide TiO_2 suspensions were photoactivated by means of UV-A radiation. Photogenerated holes and hydroxyl radicals were monitored over time by observing their selective reaction with probe compounds, iodide and terephthalic acid, respectively. TiO_2 aggregate size and structure were characterized over the reaction time. Reactive species quenching was then described by a model, accounting for radiative phenomena, TiO_2 nanoparticle aggregation and kinetic reactions. The interaction between iodide and photogenerated holes was influenced by iodide adsorption on TiO_2 surface, described by a Langmuir–Hinshelwood mechanism, whose parameters were studied as a function of TiO_2 concentration and irradiation time. Iodide oxidation was effectively simulated by modelling the reaction volume as a completely stirred two-dimensional domain, in which irradiation phenomena were described by a two-flux model and the steady state for reactive species was assumed. The kinetic parameters for iodide adsorption and oxidation were estimated and successfully validated in a different experimental setup. The same model was adapted to describe the oxidation of terephthalic acid by hydroxyl radicals. The kinetic parameters for terephthalic acid oxidation were estimated and validated, while the issues in investigating the interaction mechanisms among the involved species have been discussed. The sensitivity of operating parameters on model response was assessed and the most relevant parameters were highlighted.

* Corresponding author. Tel.: +39 02 2399 6407.
E-mail address: manuela.antonelli@polimi.it (M. Antonelli).

1. Introduction

TiO_2 photocatalysis is a promising process arising from the peculiar photoelectrochemical properties of this semiconducting metal oxide. The process has been studied for a number of applications, mainly aimed at contaminant degradation technologies and renewable energy production [1–3]. For water and wastewater treatment applications, TiO_2 photocatalysis belongs to the family of advanced oxidation processes. The absorption of photons of appropriate wavelength ($\lambda < 390$ nm) leads to the formation of electron–hole pairs, which can migrate to the surface of the photocatalyst. When in the presence of water and oxygen molecules, this results in the production of reactive oxygen species (ROS), such as hydroxyl radicals and superoxide radical anions [4,5]. The potential of these highly reactive, non-selective species has been reported in previous research for the inactivation of pathogens and the degradation of persistent organic pollutants, such as solvents, dyes, pesticides, pharmaceuticals and personal care products, *inter alia* [6,7]. Despite such interest, the process is still not an established technology, and research efforts continue to seek to develop sustainable technological applications.

Experimental protocols for the measurement of reactive species have been developed, allowing for the monitoring of ROS generation by means of molecular probes, highly selective chemicals whose reaction products can be easily quantified by spectrophotometric and fluorimetric measures [8–12]. The application of these protocols to TiO_2 photocatalysis represents an effective tool to directly assess reactivity and to further increase the knowl-edge about complex chemical–physical interaction mechanisms, whose comprehension otherwise usually relies on the study of the degradation of model pollutants, reacting simultaneously with different species [13–15].

Regarding photocatalysis by TiO_2 dispersions, reactivity depends strongly on nanoparticle aggregation size and structure [16,17]. When TiO_2 aggregates undergo photoactivation, particles on the inside of the aggregate are effectively shielded from illumination. The extent to which light can penetrate decreases as aggregate density increases, and only exposed nanoparticles can generate electron–hole pairs. Of these pairs, the fraction lost due to recombination is also a function of aggregate density, as closer charges are more likely to undergo recombination [18]. In turn, aggregate size and structure are determined by aqueous matrix properties, such as ionic strength, pH, and solution chemistry [19–23].

In a previous work by Jassby et al. [17] the influence of aggregate size and structure on the generation of hydroxyl radicals by TiO_2 nanoparticle photocatalysis was studied and a good correlation was highlighted. On the other hand, the evaluation of the two main oxidizing species involved, namely photogenerated holes and hydroxyl radicals, and comprehensive modelling throughout the process time have yet to be accomplished for TiO_2 nanoparticle photocatalysis. Indeed, a description of the process in terms of reactive species generation over a geometric domain as a function of operating conditions, and independent of the target contaminants, represents a fundamental step for process engineering and its application to large-scale reactors.

The purpose of this research was to monitor the generation of photogenerated holes (h^+) and hydroxyl radicals ($OH^{\cdot}$) in TiO_2 nanoparticle photocatalysis, by observing their selective reactions with probe chemicals: iodide (dosed as potassium iodide, KI) to iodine (I_2) [10] and terephthalic acid (TA) to 2-hydroxyterephthalic acid (2-HTA), respectively [8]. Although superoxide anion radical ($O_2^{-\cdot}$), singlet oxygen (O_2) and hydroperoxyl radical (HO_2) also play a significant role in the photocatalytic process, photogenerated holes and hydroxyl radicals were studied in the present research work because they constitute the two fundamental reactive species involved. In fact, photogenerated holes are a primary product of TiO_2 photoactivation, while hydroxyl radicals are the most important oxidizing agents in advanced oxidation processes. Besides, these two reactive species are mutually related since hydroxyl radicals are produced in the reaction between photogenerated holes and hydroxide ions. P25 Aeroxide TiO_2 nanoparticle suspensions were photoactivated by means of UV-A radiation. The production of photogenerated holes and hydroxyl radicals was observed over time. A model for describing reactive species quenching by probe molecules is formulated, accounting for radiative phenomena, TiO_2 nanoparticle aggregation and kinetic reactions. The same model has been adapted for validation in a different experimental setup. Finally, the modelling of involved radical reactions is discussed, and the sensitivity of operating parameters on model response is assessed.

2. Material and methods

2.1. TiO_2 dispersions and reagent solutions

Experiments were performed on P25 Aeroxide TiO_2 nanopowder (Evonik, Germany) suspended in deionized water (DI). TiO_2 stock suspension (100 mg L^{-1}) was prepared by adding 10 mg of P25 TiO_2 to 100 mL of deionized water and mixing on magnetic stirrer for 2 min at 120 RPM. KI was purchased from Sigma–Aldrich (USA). A starch solution was prepared adding 5 g of starch (Sigma–Aldrich) to 1 L of boiling deionized water and mixing until complete dissolution. After 12 h settling, the supernatant was collected and 2.5 g of salicylic acid (Merck, USA) were dosed as preservative. TA (0.5 mM) and 2-HTA (0.125 mM) solutions were prepared by adding 16.6 mg of TA (Sigma–Aldrich) and 4.69 mg of 2-HTA (Sigma–Aldrich) in 200 mL of deionized water, adjusting pH to 7.9 by KOH (Sigma–Aldrich) and mixing on magnetic stirrer overnight.

2.2. TiO_2 aggregate characterization

TiO_2 aggregate size and structure were investigated by laser light scattering with a Mastersizer 3000 (Malvern, England). TiO_2 stock suspensions were prepared as previously described and diluted to a final concentration of 20 mg L^{-1} in deionized water, with and without 50 mM KI, to observe the effect of the probe compound on aggregate stability. Samples were continuously mixed on a magnetic stirrer (400 RPM) and in-line dynamic light scattering measurements were performed using a peristaltic pump for sample loading located downstream of the instrument. Time resolved size measurements, reported as median diameter (D_{50}) both as number weighted and unweighted intensity, were taken over 30 min. To obtain information about aggregate structure, the scattering intensity, $I(q)$, as a function of the scattering vector, q, for each sample was recorded over the same time period. The Mastersizer contains multiple detectors for the red He–Ne laser (632.8 nm) ranging in angle from 0 to 50 degrees, which allows for the simultaneous collection of scattering intensity data at vari-ous angles. Plotting the logarithm of the scattering intensity, $\log(I(q))$, versus the logarithm of the scattering vector, $\log(q)$, produces a curve containing the linear fractal region in which the intensity is exponentially proportional to D_f. Aggregate fractal dimension, D_f, is calculated as the negative slope of the linear fit of this region, and the range of q which comprises this region of linearity corresponds to the length scales over which the fractal behaviour holds [24].

2.3. TiO_2 nanoparticle reactivity measurement

TiO_2 nanoparticle reactivity measurements were performed in small beakers, in 10 mL batch reactors, continuously mixed on a magnetic stirrer (400 RPM) and irradiated at 365 nm. Experiments were carried out in UV boxes equipped with fluorescent UV lamps and thermostated at room temperature (22 ± 1 °C). Two different experimental setups were used, denoted UV1 and UV2. In UV1, samples were irradiated by a single 15 W lamp (Helios Italquartz, Italy), providing a radiation intensity (I) on the upper liquid surface of 1.8 ± 0.1 mW cm^{-2}, measured by means of a radiometer (HD9021, Delta Ohm, Italy). The geometrical characteristics of the beaker (H = 1 cm, Ø = 5.7 cm) created a liquid layer 0.4 cm in thickness when the stirring bar (3 × 10 mm) was introduced. In UV2, two 15 W lamps (TL-D 15 W BLB SLV, Philips, Netherlands) were mounted, resulting in 1.9 ± 0.1 mW cm^{-2} intensity on the surface of samples, monitored by a ILT1400 radiometer equipped with a SEL033 detector (International Light, USA). The overall thickness of the liquid layer in the beaker (H = 3.5 cm, Ø = 5 cm) was 0.5 cm. Radiation intensity as a function of emission wavelength at the upper liquid surface of samples for each setup is reported in Supplementary Data (SI1).

2.3.1. Photogenerated holes

Photogenerated hole production was evaluated in UV1 setup in three kind of experiments:

- sample irradiation for 30 min as a function of P25 TiO_2 (10, 25 and 40 mg L^{-1}) and KI (10, 30, 50, 75 and 100 mM) concentration,
- sample irradiation at different times (10, 20 and 30 min) as a function of KI concentration (10, 30, 50, 75 and 100 mM) for 40 mg L^{-1} P25 TiO_2 concentration,
- sample irradiation at different times (5, 10, 15, 20, 25 and 30 min) for 40 mg L^{-1} P25 TiO_2 and 50 mM KI concentration.

Samples were composed of variable volumes of 100 mg L^{-1} P25 TiO_2 stock suspension, 250 mM KI solution and deionized water. After irradiation, a 0.5 mL aliquot of the sample volume was collected and mixed with the starch solution (1:1 volume ratio), which was then transferred to a glass cuvette (10 mm optical path) for absorbance measurement at 585 nm vs. deionized water in spectrophotometer (UV–vis 2, Unicam, USA). Absorbance values were related to iodine concentration by a standard curve that was evaluated by spectrophotometric measurements after subtracting the TiO_2 suspension contribution from non-irradiated samples. The corresponding photogenerated holes concentration was stoichiometrically determined to be twice the produced iodine concentration, according to the following reaction:

$$2I^- + 2h^+ \rightarrow I_2 \quad (1)$$

A standard curve was determined using a 0.025 M iodine (Sigma–Aldrich, USA) stock solution that was diluted to obtain solutions at concentrations ranging between 0.00625 and 0.0625 mM (concentration step: 0.00625 mM). The absorbance of different concentrated iodine solutions was measured by a spectrophotometer with the same procedure described for irradiated samples during photocatalytic tests.

Validation tests were carried out in setup UV2 at varying times (5, 10, 15, 20, 25 and 30 min) on 20 mg L^{-1} P25 TiO_2 and 50 mM KI concentration samples. The same procedure was used and measures of absorbance were performed with a Cary 100 spectrophotometer (Agilent, USA).

Tests were replicated at least three times for each combination of conditions.

2.3.2. Hydroxyl radicals

Hydroxyl radical production tests were performed in setup UV1 on samples containing 40 mg L^{-1} P25 TiO_2 and 0.125 mM TA. Samples, comprised of 4 mL of 100 mg L^{-1} P25 TiO_2 stock solution, 2.5 mL of 0.5 mM TA solution and 1 mL of deionized water, were irradiated for 5, 10, 15, 20, 25 and 30 min. After irradiation, 0.5 mL of the volume was sampled, diluted to 1.25 mL with deionized water and centrifuged at 12,000 RPM for 5 min in order to separate TiO_2 aggregates. Then, 1 mL of supernatant was removed and transferred to a plastic cuvette (10 mm optical path) for fluorescence measurement (excitation at 315 nm and emission at 425 nm) by means of a Varian Eclipse fluorometer (Agilent). Fluorescence values were related to 2-HTA concentration by a standard curve. The corresponding hydroxyl radical concentration was estimated by the following reaction, assuming that trapping efficiency for $OH^{\cdot}$ radicals by TA is 80% [25]:

$$TA + OH^{\cdot} \rightarrow 2\text{-HTA} \quad (2)$$

The standard curve was determined using a 0.125 mM 2-HTA stock solution that was diluted to obtain solutions at concentrations ranging between 0.00125 and 0.0125 mM (concentration step: 0.00125 mM). The fluorescence of different concentrations of 2-HTA solutions was measured as well as for irradiated samples during photocatalytic tests.

Validation tests were carried out in UV2 setup at different times (5, 10, 15, 20, 25 and 30 min) on samples containing 20 mg L^{-1} P25 TiO_2 and 125 mM TA.

Measures were repeated at least thrice for each combination of operating conditions.

3. Results and discussion

3.1. TiO_2 aggregate characterization

Measurement conditions were designed to mimic the setup for reactivity measurements. TiO_2 aggregate size evolution was tracked for 30 min and, as can be seen in Supplementary Data (SI2), samples in deionized water were stable with a number weighted D_{50} of 114 ± 0.5 nm over the process time. The unweighted D_{50} indicated an increase from 3.28 ± 0.269 μm initially to 4.17 ± 0.431 μm after 30 min. The difference in these values reflects the high polydispersity of TiO_2 suspensions, result-ing from the dispersion method. However, the initial number weighted values are all sharply centered around 114 nm indicating that the vast majority of aggregates exist at this smaller size class with relatively few large aggregates influencing the unweighted average size. Samples that were destabilized from the addition of KI (50 mM) showed an increase in the number weighted D_{50} from 111 ± 1.6 nm initially to 681 ± 58.7 nm after 30 min, with unweighted D_{50} increasing from 3.45 ± 0.261 to 12.17 ± 0.451 μm. Structure calculations yielded a D_f of 2.17 ± 0.024 for P25 in deionized water which remained unchanged over the 30 min. The range of q values for which the scattering response was linear corresponded to length scales ranging from 660 nm to 3.4 μm. These values are consistent with the fractal dimensions reported for P25 by Jassby et al. [17].

3.2. TiO_2 nanoparticle reactivity measurement

TiO_2 nanoparticle reactivity tests were carried out in an experimental setup minimizing sample volume and liquid layer thickness so that samples were irradiated as uniformly as possible. Due to the small liquid volume pH and temperature were not monitored over time during irradiation. The pH of TiO_2 suspensions, measured in larger volumes of non-reacted samples, was 6.3 ± 0.1 for

photogenerated hole tests and 7.9 ± 0.1 for hydroxyl radical tests. The latter value is higher due to pH adjustment by KOH to allow for the dissolution of TA. For both probe compounds it was verified that no significant oxidation phenomena were determined by photolysis over the whole process time (30 min).

3.2.1. Photogenerated holes

The influence of the initial KI concentration on photogenerated hole production was studied at a fixed irradiation time (30 min) for varying P25 TiO_2 concentrations (10, 25 and 40 mg L^{-1}), and at varying irradiation times (10, 20 and 30 min) for a fixed P25 TiO_2 concentration (40 mg L^{-1}). Experimental results are shown in Figs. 1 and 2.

For the same KI concentration, an increase in oxidized iodide concentration was observed when increasing the P25 TiO_2 concentration (Fig. 1). This result suggests that a greater amount of photocatalyst involves higher radiation absorption, a greater number of active sites and overall higher photoreactivity, in agreement with Chong et al. [2].

Moreover, independently from irradiation time (Fig. 2), an increase in photogenerated hole concentration with KI concentration was observed at a fixed P25 TiO_2 concentration, despite the presence of the molecular probe in excess. This behaviour reveals that the reaction between iodide and photogenerated holes is significantly affected by the diffusion of iodide onto nanoparticle surface. Therefore, the effectiveness of the method in quantifying photogenerated holes is strictly related to KI concentration, as previously discussed in Herrmann and Pichat [26], by which the oxidation mechanism of iodide was supposed to depend on iodide adsorption on TiO_2 surface, according to a Langmuir type model. Consequently, the interaction between iodide and photogenerated

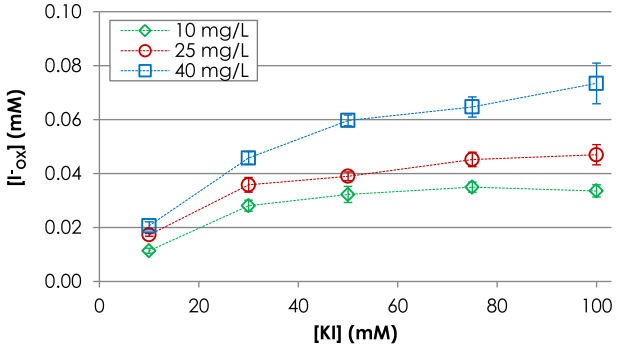

Fig. 1. Oxidized iodide vs. KI concentration at different TiO_2 concentrations (30 min irradiation time, UV1 setup).

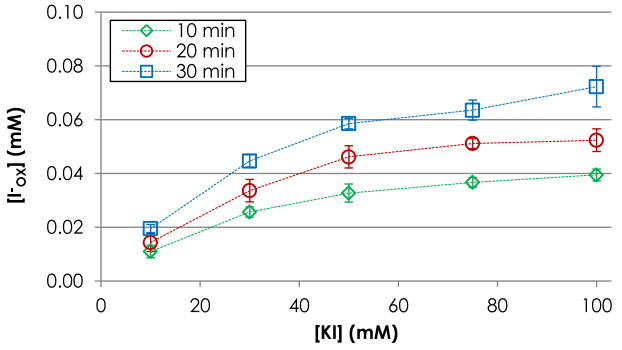

Fig. 2. Oxidized iodide vs. KI concentration at different irradiation times ([TiO_2] = 40 mg L^{-1}, UV1 setup).

Table 1
Estimated values of K_A and K_R vs. P25 TiO_2 concentration and irradiation time interval (Δt).

[TiO_2] (mg L^{-1})	Δt (min)	K_A (M^{-1})	K_R (M s^{-1})	R^2
10	30	91.03	2.15E-08	0.905
25	30	64.27	2.97E-08	0.937
40	10	33.20	8.60E-08	0.998
	20	28.61	6.18E-08	0.963
	30	29.62	5.30E-08	0.986

holes has been described by a Langmuir–Hinshelwood (LH) mecha-nism [26]:

$$r = \frac{d[I^-]}{dt} = -K_R \cdot \theta_{I^-} = -K_R \cdot \frac{K_A[I^-]}{1 + K_A[I^-]} \quad (3)$$

in which r is the reaction rate, [I^-] is the concentration of iodide, θ_{I^-} is the surface coverage, K_A is the equilibrium constant of adsorption and K_R is the LH reaction constant.

The values of LH coefficients, K_A and K_R, can be estimated by the method of initial rates [27] using experimental results shown in Figs. 1 and 2, see Supplementary Data (SI3). Parameters estimated by linear regression are shown in Table 1. The coefficients of determination (R^2) of the linear regressions are higher than 0.905, indicating that the LH model is effective in data description. A linear decreasing trend (R^2 = 0.995) was observed for K_A with increasing TiO_2 concentration (for the same time interval, 30 min). This is expected as the equilibrium constant of adsorption is inversely related to the availability of adsorption sites on TiO_2 aggregates, which is a function of the photocatalyst surface [28]. An increasing trend with TiO_2 concentration was determined for K_R at the same time interval (30 min), which is probably due to the enhanced photocatalytic properties of concentrated TiO_2 suspensions in terms of absorption of incident radiation and number of active sites. As reported by Xu and Langford [29], the estimation of parameters strongly depends on the irradiation time interval chosen for the initial reaction rate calculation, particularly when the operative conditions that affect adsorption and reaction mechanisms change over time. Different time intervals (10, 20 and 30 min) were considered here depending on experimental conditions. For fixed TiO_2 concentration (40 mg L^{-1}) and different irradiation times, K_A maintained a nearly constant value and K_R strongly decreased with time interval. This K_R trend is unexpected and is discussed in Section 3.3.3.

Experimental results illustrate the strong dependence on the method for photogenerated hole measurement from photocatalyst and probe concentrations. Therefore experiments for the evaluation of photogenerated hole production over 30 min irradiation time were performed with TiO_2 and KI concentrations fixed at 40 mg L^{-1} and 50 mM, respectively, as this was proved to be the best combination. In Fig. 3, oxidized iodide concentration as a func-tion of irradiation time is reported (EXP – UV1). An increasing trend with decreasing slope over time for oxidized iodide was observed in contrast to the normally expected true zero order kinetics for oxidation reactions without interferences. According to Herrmann and Pichat [26], this behaviour is due to light absorp-tion by iodine in solution, whose contribution in terms of absor-bance is significant even at small amounts. The oxidized iodide concentration trend over time will be discussed in Section 3.3.3.

3.2.2. Hydroxyl radicals

2-HTA concentrations, corresponding to the oxidation of TA by hydroxyl radicals, as a function of irradiation time (EXP – UV1) are shown in Fig. 4. Similarly to holes, hydroxyl radical production showed an increasing trend with decreasing slope over time, as later discussed in Section 3.3.3.

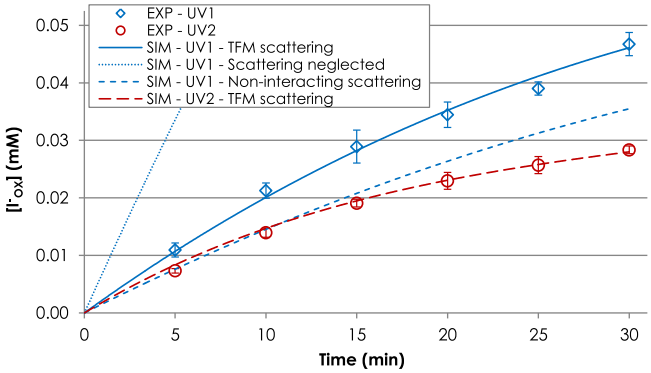

Fig. 3. Oxidized iodide concentration vs. time: experimental data obtained in UV1 (diamonds) and UV2 (circles) setup, simulated data obtained in UV1 and UV2 setup using different scattering models.

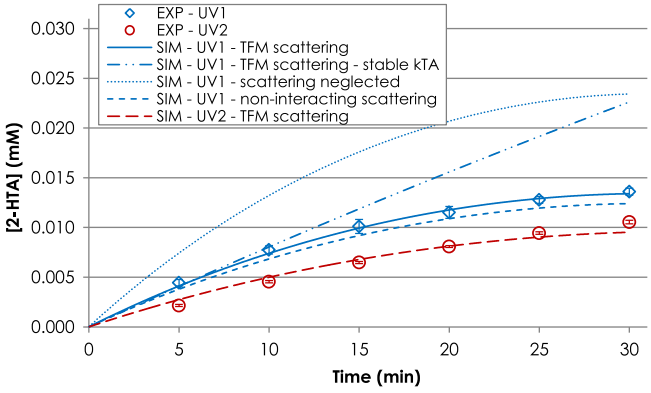

Fig. 4. 2-HTA concentration vs. time: experimental data obtained in UV1 (diamonds) and UV2 (circles) setup, simulated data obtained in UV1 and UV2 setup using different scattering models.

3.3. TiO_2 nanoparticle photocatalysis modelling

Modelling criteria proposed in the literature for TiO_2 photocatalysis were adopted and implemented for describing a transient system over the experimental geometric domain. The reactivity measurement setup was modelled as a two-dimensional completely stirred reactor, taking into account both the optical and chemical phenomena involved. The model considers chemical species evolution over time under the assumption of steady state for reactive species [30], as their generation and decay times are several orders of magnitude smaller than those of other species [31]. The proposed irradiation model was developed in order to describe the change in optical properties over time, while the adopted kinetic model accounts for the influence of TiO_2 nanoparticle aggregate size and structure on process yields, as proposed by Jassby et al. [17].

3.3.1. Irradiation model

The irradiation model calculates the number of photons absorbed by the photocatalyst per unit of volume in the unit of time, $R(t)$, which is reported in the literature in several ways, including as local volumetric rate of photon absorption (LVRPA), *inter alia* [15,32]. This parameter is a function of time since the optical properties of the aqueous solution change during the process and it was evaluated for the experimental setup as reported in Eq. (4):

$$R(t) = \int_{\lambda} \frac{I_{ABS}(\lambda, t) S}{h\nu(\lambda) N_A} d\lambda \qquad (4)$$

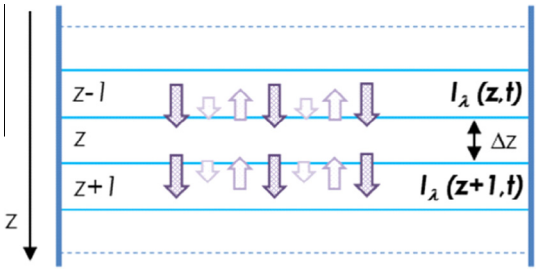

Fig. 5. 2D-domain scheme of the reactor. For a generic layer, incoming radiation intensity (I_λ) is given by the sum of UV lamp direct emission and back-scattering contributions.

in which $I_{ABS}(\lambda)$ is the radiation intensity per unit surface absorbed by TiO_2 suspension at a given wavelength in a time step, S is the irradiated surface (25.52 cm^2 and 19.63 cm^2 in UV1 and UV2 setup respectively), $h\nu(\lambda)$ is the energy of a photon at a given wavelength and N_A is the Avogadro's number. For describing the radiation transmission, the total liquid height was divided into layers (z) of equal thickness (Δz = 0.2 mm), as illustrated in Fig. 5. The number of layers was 20 in setup UV1 and 25 in setup UV2.

The first layer was assumed to be irradiated vertically, while the radiation intensity absorbed by the TiO_2 suspension ($I_{ABS,\lambda}$) in a generic layer z for a given wavelength at each time step per unit surface was calculated by the following expression, derived from the Beer–Lambert law:

$$I_{ABS,\lambda}(z,t) = I_\lambda(z,t) \cdot 10^{-ABS_{SOL,\lambda}(t)} \cdot \left(1 - 10^{-(1-\alpha_\lambda)EXT_{TiO_2,\lambda}(t)}\right) \qquad (5)$$

in which $ABS_{SOL,\lambda}(t)$ is the volumetric absorbance of the aqueous solution without considering the presence of TiO_2 nanoparticles, $EXT_{TiO_2,\lambda}(t)$ is the volumetric extinction of TiO_2 suspension, accounting for the coexistence of absorption and scattering phenomena, and α_λ is the scattering albedo at a given wavelength [33]. These terms were considered to be identical throughout the liquid volume at any given time step under the assumption of continuous mixing during irradiation. In the present model, specific absorption and scattering coefficients as a function of wavelength reported by Satuf et al. [34] for P25 TiO_2 were used for determining albedo coefficients and discriminating between the two components in spectrophotometric measures.

I_λ is the incoming radiation intensity in each layer, given by the sum of the radiative contribution from the other layers. In detail, radiation scattering was described by a two-flux model (TFM) [33,35], in which TiO_2 nanoparticle backscattering is introduced, hence the presence of vertical radiative terms in addition to the radiation transmitted from the upper layers and resulting from the direct emission of UV lamps. The total radiation intensity per unit volume (R) was calculated as the sum of the contributions of all the liquid layers $R(t)$ at each step time.

In modelling photogenerated hole production, both absorbance by the aqueous solution and extinction by the TiO_2 suspension were considered to change over time: in the first case due to the production of iodine and in the second because of TiO_2 aggregation mechanisms. The values of $ABS_{SOL,\lambda}(t)$ during process time were obtained by means of absorbance measures of different concentrated iodine solutions (Supplementary Data, SI4), and the time-dependent values of $EXT_{TiO_2,\lambda}(t)$ were determined by spectrophotometric measures of KI solutions containing P25 TiO_2 in suspension (Supplementary Data, SI5). In modelling hydroxyl radical production, no significant modifications, neither in aqueous solution absorbance nor in TiO_2 suspension extinction, were observed over time, as reported in the Supplementary Data (SI6).

3.3.2. Kinetic model

The equations for the variation of the concentration of photogenerated holes, promoted electrons and hydroxyl radicals over time were derived from the literature [17,36,37] and experimental results:

$$\frac{d[h^+]}{dt} = \Phi R - k_1[h^+][OH^-] - \varepsilon^{D_f-1}k_2[h^+][e^-] - k_3[h^+][OH^\cdot] - \left\{k_R[h^+]\frac{K_A[I^-]}{1+K_A[I^-]}\right\} \quad (6)$$

$$\frac{d[e^-]}{dt} = \Phi R - \varepsilon^{D_f-1}k_2[h^+][e^-] - k_4[e^-][OH^\cdot] - k_5[e^-][O_2] \quad (7)$$

$$\frac{d[OH^\cdot]}{dt} = k_1[h^+][OH^-] - k_3[OH^\cdot][h^+] - k_4[OH^\cdot][e^-] - k_6[OH^\cdot]^2 - \{k_{TA}[OH^\cdot][TA]\} \quad (8)$$

in which Φ is the quantum yield of the material and R is the radiation intensity per unit volume. $[h^+]$, $[e^-]$, $[OH^-]$, $[OH^\cdot]$, $[I^-]$, $[O_2]$ and [TA] are the molar concentrations of photogenerated holes, promoted electrons, hydroxyl ions, hydroxyl radicals, iodide ions, dissolved oxygen and TA, respectively. k_1, k_2 and k_3 are rate constants for reactions of photogenerated holes with hydroxide ions, promoted electrons and hydroxyl radicals, respectively. k_4 and k_5 are rate constants for reactions of promoted electrons with hydroxyl radicals and dissolved oxygen. k_6 is the rate constant for the self-quenching of hydroxyl radicals and k_{TA} is the rate constants for the reaction of hydroxyl radicals and TA. Regarding TiO_2 aggregate characteristics, ε^{D_f-1} is the parameter that describes the structural characteristics of TiO_2 nanoparticles aggregates, where ε is the porosity and D_f is the fractal dimension of TiO_2 aggregates, and which depends on TiO_2 aggregate hydrodynamic radius (R_h) and on TiO_2 nanoparticle primary radius (R_p) [17,18].

In Eq. (6) the first term on the right side represents photogenerated hole production, the second the hydroxyl radical production, the third the electron–hole recombination and the fourth the reaction between photogenerated holes and hydroxyl radicals. The fifth term refers to the quenching of photogenerated holes by iodide ions adsorbed on TiO_2 nanoparticle surface, assuming that the reaction between iodide and photogenerated holes is described by the Langmuir–Hinshelwood mechanism as discussed previously (Section 3.2.1). The reaction constant between iodide and photogenerated holes, previously expressed as K_R (Eq. (3)), is reported in Eq. (6) as the product between the photogenerated hole concentration and an intrinsic kinetic constant k_R (s^{-1}), showing the direct dependence of the reaction rate on the concentration of photogenerated holes:

$$K_R = k_R[h^+] \quad (9)$$

Hence, unlike K_R, the kinetic constant, k_R, is independent from the available photogenerated hole concentration. It is not affected by operating conditions, and it is time-invariant.

In Eq. (7) the first two terms on the right side represent promoted electrons production and recombination, the third the reaction between promoted electrons and hydroxyl radicals and the fourth represents superoxide radical production.

In Eq. (8) the first term on the right side represents hydroxyl radicals generation, the second and the third terms the interaction of hydroxyl radicals with photogenerated holes and promoted electrons, the fourth the hydroxyl radical self-quenching, and the fifth term the quenching of hydroxyl radicals by TA.

In Eqs. (6) and (8), terms reported in brackets have to be considered only if iodide and TA are present in solution.

Photogenerated hole, promoted electron, and hydroxyl radical concentrations can be calculated at steady state by equating the accumulation of the reactive species over time to zero, which leads to the expressions for the reactive species reported in Supplementary Data (SI7).

In the described system the iodine production over time can be expressed by Eq. (10):

$$\frac{d[I_2]}{dt} = \frac{1}{2}\cdot k_R\cdot[h^+]_{SS}\cdot\theta_{I^-} = \frac{1}{2}\cdot k_R\cdot[h^+]_{SS}\cdot\frac{K_A[I^-]}{1+K_A[I^-]} \quad (10)$$

On the other hand, the 2-HTA production over time can be evaluated as:

$$\frac{d[2\text{-HTA}]}{dt} = k_{TA}[OH^\cdot]_{SS}[TA] \quad (11)$$

The production of iodine and 2-HTA was estimated by solving and integrating the equations over the process time (30 min) with a step time of 1 s. The time-independence of the model at this time step was verified.

The values for kinetic constants used in modelling are reported in the Supplementary Data (SI8), while the values for equilibrium adsorption constant K_A were derived from Table 1. Experimental values for R_h and D_f were experimentally determined in Section 3.1, R_p was provided by the manufacturer (~20÷25 nm), while ε was calculated according to the following equation [18]:

$$\varepsilon = R_h^{D_f-3}R_p^{3-D_f} \quad (12)$$

Reaction kinetic constants k_R and k_{TA}, characteristic of the iodide oxidation and TA hydroxylation reactions, were determined from the two kinetic models (Eqs. (10) and (11)) by a least-square optimization procedure, that resulted in the best fitting of experimental data obtained in setup UV1. The validation of kinetic models was carried out using experimental results obtained in setup UV2.

3.3.3. Modelling results and sensitivity analysis

The simulated production of I_2 and 2-HTA over time is reported in Figs. 3 and 4 (SIM – UV1 – TFM scattering) in comparison with respective experimental results obtained in setup UV1 (EXP – UV1). The values of R, $[h^+]_{SS}$ and $[OH^\cdot]_{SS}$ calculated by the model after 1 and 30 min process time for setup UV1 are given in Table 2.

Model calculations of iodide oxidation by photogenerated holes based on the calculated radiation intensity per unit volume (R) shows a strong decrease (−60%) after 30 min irradiation time; the reason for this significant reduction in the radiation absorbed by TiO_2 suspension is that the energy balance is modified over time by generated iodine in solution, absorbing an increasing amount of radiation, and by aggregation of TiO_2 particles, lowering the absorbance of the TiO_2 suspension (Supplementary Data, SI4 and SI5). These factors explain the observed slowdown trend in iodide oxidation. As a consequence, the concentrations of photogenerated holes and hydroxyl radicals at the steady state decrease over process time of 60% and 29%, respectively.

Conversely, no energy balance changes are considered in the model describing TA hydroxylation by hydroxyl radicals, so that R and $[h^+]_{SS}$ are constant over process time. $[OH^\cdot]_{SS}$ slightly increases during 30 min (+1%) because of the decrease in TA concentration over process time (−11%).

The optimum estimated value for k_R was 8.25 s^{-1}, while linearly decreasing values for k_{TA} from 9.89E03 M^{-1} s^{-1} to 3.96E02 M^{-1} s^{-1} over time resulted in a satisfactory fitting of experimental data. These kinetic parameters yielded R^2 values equal to 0.991 and 0.993 for iodide and TA oxidation, respectively. A variable k_{TA} value was adopted because it provides a better fit with respect to any fixed k_{TA} value, since the strong curvature of experimental data is not predicted otherwise, as can be seen in Fig. 4 (SIM – UV1 –TFM scattering – stable k_{TA}). The latter simulation was run with a

Table 2
Values of R, $[h^+]_{SS}$, and $[OH^\cdot]_{SS}$ calculated by models after 1 and 30 min process time. Simulated data relative to both experimental setup (UV1 and UV2, used for parameter calibration and validation, respectively) and both models are reported.

Simulated process	h^+ quenching by I^-				OH· quenching by TA			
Experimental setup	UV1		UV2		UV1		UV2	
Time step (min)	1	30	1	30	1	30	1	30
R (Einstein L^{-1} s^{-1})	4.08E-05	1.60E-05	3.40E-05	7.24E-06	4.29E-05		2.23E-05	
$[h^+]_{SS}$ (M)	8.68E-09	3.41E-09	5.26E-09	1.54E-09	2.70E-10		1.40E-09	
$[OH^\cdot]_{SS}$ (M)	6.08E-09	4.29E+09	5.08E-09	3.08E-09	1.22E-08	1.23E-08	8.05E-09	8.14E-09

k_{TA} value fixed at 9.07E03 M^{-1} s^{-1}, which gave the best match with the initial trend of experimental data.

For a comparison with experimental data reported in Figs. 1 and 2, the Langmuir–Hinshelwood kinetic constant K_R was calculated over time according to Eq. (9), i.e. as the product between k_R, estimated by the optimization procedure, and $[h^+]_{SS}$, obtaining values decreasing from 6.29E-08 M s^{-1} to 2.47E-08 M s^{-1} over process time, comparable to data in Table 1. The change in $[h^+]_{SS}$ over process time probably explains the experimental K_R kinetic constant decrease reported in Table 1 at different irradiation time intervals.

Given the limitations of the method adopted in Section 3.2.1 for parameter estimation, the agreement between observed and simulated K_R kinetic constant values can be considered satisfactory. On the other hand, the kinetic constant for TA hydroxylation, k_{TA}, estimated here is significantly different from the value proposed in literature, namely 3.30E9 M^{-1} s^{-1} [38]. This discrepancy can be explained assuming that, in a heterogeneous system such as the present one, the TA reaction with hydroxyl radicals could be limited by diffusion on the TiO_2 surface, which is in turn impeded by the pH of solution (higher than the point of zero charge for TiO_2) and by hydroxyl radical effective availability for probe com-pound hydroxylation. Moreover, the reactivity coefficient reported in literature was estimated in a homogeneous system in which hydroxyl radicals were generated by means of water radiolysis. As already discussed, k_{TA} modification over process time was assumed to reproduce the decreasing trend of experimental data not otherwise described by the model. The model parameters that change over time and that may determine its curvature are TA concentration and solution pH. Regarding TA concentration, its observed slight decrease cannot explain the saturation trend of experimental data for 2-HTA production, since its value does not become limiting for the process. Although it is not monitored throughout the experiment, several simulations were performed at varying pH, however a decreasing trend similar to that shown by experimental data was not observed. Hence, the experimental trend that can be effectively modelled by assuming a linear decrease in TA reactivity over process time is probably due to the changing nature of the interaction between TA and hydroxyl radicals or to modifications in surface chemistry, not related to the morphology of TiO_2 aggregates that was stable over time. Further research should be devoted to the study of the hydroxylation of TA by hydroxyl radicals, possibly involving the use of analytical techniques for monitoring the generation of radical species, such as electron paramagnetic resonance (EPR).

Photogenerated hole and hydroxyl radical consumption by different reactions was assessed on the basis of kinetic constants and concentrations of compounds in solution: in the kinetic model describing iodide oxidation, most of the photogenerated holes are self-quenched in the reaction with promoted electrons (96.8%), some react with hydroxyl ions in the formation of hydro-xyl radicals (1.9%) and a fraction is lost in recombination with hydroxyl radicals (1.1%). Only 0.2% of photogenerated holes oxidize iodide in solution. These shares do not change significantly throughout the experiment. The strong detrimental effect of electron–hole recombination on process yield is clear, as this phenomenon is one of the main drawbacks of TiO_2 photocatalysis, whose reduction has been discussed in a number of published papers [39,40]. In the kinetic model describing TA hydroxylation, most of hydroxyl radicals are lost to self-quenching (rising from 95.5% to 99.5% in 30 min), while a lower fraction of hydroxyl radicals react with TA. This latter fraction is significantly reduced at the end of the process time, falling from 1.8% to 0.01%, due to the decrease in TA concentration, although this change is not sufficient to explain the strong curvature of experimental data. The fraction of hydroxyl radicals reacting with photogenerated holes is 2.7%at the beginning and 0.5% at the end of the process time, while the reaction with promoted electrons is negligible.

Many authors have pointed out that TiO_2 photocatalysis modelling strongly depends on the evaluation of the volumetric rate of photon absorption, since it represents a fundamental step for the process. In particular, several works highlighted the importance of modelling TiO_2 nanoparticle scattering in a slurry reactor, and some formulations for its accurate description have been proposed [15,32]. Two irradiation models have been implemented in addition to that already introduced, one neglecting scattering and a second assuming that radiation no longer interacts with TiO_2 suspension after being scattered once. Results for the UV1 setup are reported in Figs. 3 and 4, while similar results were obtained for UV2 setup, here not shown. When light scattering is neglected, the amount of photons absorbed by TiO_2 nanoparticles is abundantly over-estimated, resulting in higher I_2 or 2-HTA production (SIM – UV1 –Scattering neglected). Instead, when the absorption of the scattered radiation is not considered, the rate of photon absorption is under-estimated (SIM – UV1 – Non-interacting scattering). Hence, a proper consideration of scattering phenomena is fundamental in describing TiO_2 nanoparticles photocatalysis. However, only the photogener-ated hole model is strongly affected by scattering, while the differ-ences are less marked in the hydroxyl radical model, probably due to intermediate reactions acting as a limiting step in TA hydrox-ylation and reducing the direct influence of radiative phenomena.

Kinetic constants k_R and k_{TA}, determined by a least-squares optimization procedure, were validated using data obtained under different experimental conditions (UV2 setup). The values of R, $[h^+]_{SS}$ and $[OH^\cdot]_{SS}$ after 1 and 30 min process time for UV2 setup are reported in Table 2.

Figs. 3 and 4 show that simulated data for the production of I_2 and 2-HTA over process time (SIM – UV2 – TFM scattering), running the relative kinetic model with the k_R and k_{TA} values pre-viously determined, effectively fit the data obtained under differ-ent experimental conditions (EXP - UV2), giving R^2 values equal to 0.994 and 0.962 for iodide and TA oxidation, respectively. The high correspondence observed suggests that both the irradiation and the kinetic model proposed are effective in modelling TiO_2 photocatalysis. However, while the model consistently describes the phenomena related to iodide oxidation by photogenerated holes, it is less reliable for modelling TA hydroxylation by hydroxyl radicals, since the choice of the optimal kinetic parameters, differing from those reported in literature and time-varying,

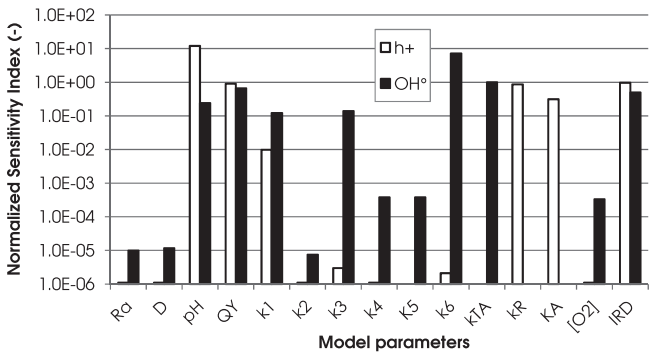

Fig. 6. Local sensitivity analysis of the parameters of the models for photogenerated holes and hydroxyl radicals production: Normalized Sensitivity Index (NSI) was calculated as the ratio between percentage variation of model outputs and respective parameter values. QY is the quantum yield.

cannot be explained on the basis of involved phenomena and could be due to some neglected mechanisms.

The sensitivity assessment of operating parameters was performed by means of a local sensitivity analysis method, varying one parameter at a time and keeping the others fixed [41]. This methodology was used since all the analysed parameters are independent. Results are reported in Fig. 6, while more details about sensitivity analysis are given in the Supplementary Data (SI9).

For the model describing photogenerated hole quenching by iodide, the most important parameters affecting the photocatalytic process are pH, radiation intensity, quantum yield, k_R and K_A. TiO_2 aggregates size and structure slightly affect the process, although in the literature these features are described as an important driver for the recombination of electron–hole pairs [17,18].

The most important role of TiO_2 aggregates structure concerns the effects on optical phenomena (absorption, scattering) and it is accounted for in the irradiation model. The strong importance of k_R and K_A is probably distorted by the experimental methodology, involving iodine measurements. For the model describing hydroxyl radicals quenching by TA, the sensitivity analysis indicated that k_6, k_{TA}, quantum yield and radiation intensity are the most important parameters for photocatalysis.

In summary, the reported modelling procedure, integrating the insights of several previous research works with recent protocols for the measurement of reactive species, represents a significant step forward in the description of TiO_2 nanoparticle photocatalysis. The main advantages of the proposed method, whose effectiveness in reproducing time series has been validated in a separate experimental setup, are the independence from the model compound, the estimation of the concentration of the individual reactive species and the potential adaptability to different reactor configurations. Further developments may provide for the implementation of more advanced optical and fluid-dynamic models by means of powerful computational tools, e.g. CFD codes, so that more complex configurations could be described. Additionally, the present model, by means of an adequate adaptation, even in terms of other probe com-pounds adopted instead of KI and TA, could be extended to predict:(1) the production of other reactive species, as superoxide anion radical, singlet oxygen and hydroperoxyl radical, (2) the degradation of priority contaminants in water and wastewater, (3) the influence of other compounds, such as inorganic ions, usually competing for the consumption of reactive species and adversely affecting process yields.

4. Conclusions

Two experimental protocols for the measurement of reactive species, namely photogenerated holes and hydroxyl radicals, were successfully applied to the experimental setup. The interaction between iodide and photogenerated holes depended on iodide adsorption on TiO_2 surface, that was described by a Langmuir–Hinshelwood mechanism, whose parameters were studied as a function of TiO_2 concentration and irradiation time. Iodide oxidation was effectively simulated by modelling the reaction volume as a completely stirred two-dimensional domain, in which irradiation phenomena were described by a two-flux model and the steady state for reactive species was assumed. The kinetic parameters for iodide adsorption and oxidation were estimated and successfully validated in a different experimental setup. The same model was adapted to describe the oxidation of terephthalic acid by hydroxyl radicals. The kinetic parameters for terephthalic acid oxidation were estimated and validated, while the issues in investigating the interaction mechanisms among the involved species have been discussed. The sensitivity of operating parameters on model response was assessed and the most relevant parameters were highlighted.

The present work represents a significant advance in the understanding of fundamental chemical-physical processes involved in reactive species generation as well as it provides a valuable modelling methodology accounting for radiation transfer and chemical reactions.

Acknowledgements

Funding for JFB was gratefully provided by the NIEHS-supported Duke University Superfund Research Center (NIEHS grant P42-ES010356).

Appendix A. Supplementary data

Supplementary data associated with this article can be found, in the online version.

References

[1] O. Carp, Photoinduced reactivity of titanium dioxide, Prog. Solid State Chem. 32 (2004) 33–177.
[2] M.N. Chong, B. Jin, C.W.K. Chow, C. Saint, Recent developments in photocatalytic water treatment technology: a review, Water Res. 44 (2010) 2997–3027.
[3] T. Ochiai, A. Fujishima, Photoelectrochemical properties of TiO_2 photocatalyst and its applications for environmental purification, J. Photochem. Photobiol. C Photochem. Rev. 13 (2012) 247–262.
[4] B. Ohtani, Photocatalysis A to Z—what we know and what we do not know in a scientific sense, J. Photochem. Photobiol. C Photochem. Rev. 11 (2010) 157–178.
[5] P. Pichat, Photocatalysis and water purification: from fundamentals to recent applications, Wiley-VCH, 2013.
[6] S. Malato, P. Fernández-Ibáñez, M.I.I. Maldonado, J. Blanco, W. Gernjak, Decontamination and disinfection of water by solar photocatalysis: recent overview and trends, Catal. Today. 147 (2009) 1–59.
[7] H. Choi, S.R. Al-Abed, D.D. Dionysiou, E. Stathatos, P. Lianos, TiO_2-based advanced oxidation nanotechnologies for water purification and reuse, Sustain. Sci. Eng. 2 (2010) 229–254.
[8] K.I. Ishibashi, A. Fujishima, T. Watanabe, K. Hashimoto, Detection of active oxidative species in TiO_2 photocatalysis using the fluorescence technique, Electrochem. Commun. 2 (2000) 207–210.
[9] T. Hirakawa, K. Yawata, Y. Nosaka, Photocatalytic reactivity for O_2^- and $OH^\cdot$ radical formation in anatase and rutile TiO_2 suspension as the effect of H_2O_2 addition, Appl. Catal. A Gen. 325 (2007) 105–111.
[10] S.H. Yoon, J.H. Lee, Oxidation mechanism of As(III) in the UV/TiO_2 system: evidence for a direct hole oxidation mechanism, Environ. Sci. Technol. 39 (2005) 9695–9701.
[11] G. Bartosz, Use of spectroscopic probes for detection of reactive oxygen species, Clin. Chim. Acta. 368 (2006) 53–76.
[12] N. Soh, Recent advances in fluorescent probes for the detection of reactive oxygen species, Anal. Bioanal. Chem. 386 (2006) 532–543.
[13] M.L. Satuf, R.J. Brandi, A.E. Cassano, O.M. Alfano, Photocatalytic degradation of 4-chlorophenol: a kinetic study, Appl. Catal. B Environ. 82 (2008) 37–49.
[14] M. Vezzoli, W.N. Martens, J.M. Bell, Investigation of phenol degradation: true reaction kinetics on fixed film titanium dioxide photocatalyst, Appl. Catal. A Gen. 404 (2011) 155–163.

[15] I. Grčić, G. Li, Puma, Photocatalytic degradation of water contaminants in multiple photoreactors and evaluation of reaction kinetic constants independent of photon absorption, irradiance, reactor geometry, and hydrodynamics, Environ. Sci. Technol. 47 (2013) 13702–13711.
[16] H. Lin, C. Huang, W. Li, C. Ni, S. Shah, Y. Tseng, Size dependency of nanocrystalline TiO_2 on its optical property and photocatalytic reactivity exemplified by 2-chlorophenol, Appl. Catal. B Environ. 68 (2006) 1–11.
[17] D. Jassby, J.F. Budarz, M. Wiesner, Impact of aggregate size and structure on the photocatalytic properties of TiO_2 and ZnO nanoparticles, Environ. Sci. Technol. 46 (2012) 6934–6941.
[18] E.M. Hotze, J.Y. Bottero, M.R. Wiesner, Theoretical framework for nanoparticle reactivity as a function of aggregation state, Langmuir 26 (2010) 11170–11175.
[19] J. Jiang, G. Oberdörster, P. Biswas, Characterization of size, surface charge, and agglomeration state of nanoparticle dispersions for toxicological studies, J. Nanoparticle Res. 11 (2008) 77–89.
[20] A.A. Keller, H. Wang, D. Zhou, H.S. Lenihan, G. Cherr, B.J. Cardinale, Stability and aggregation of metal oxide nanoparticles in natural aqueous matrices, Environ. Sci. Technol. 44 (2010) 1962–1967.
[21] E.M. Hotze, T. Phenrat, G.V. Lowry, Nanoparticle aggregation: challenges to understanding transport and reactivity in the environment, J. Environ. Qual. 39 (2010) 1909.
[22] Y.H. Shih, W.S. Liu, Y.F. Su, Aggregation of stabilized TiO_2 nanoparticle suspensions in the presence of inorganic ions, Environ. Toxicol. Chem. 31 (2012) 1693–1698.
[23] Y.H. Shih, C.M. Zhuang, C.P. Tso, C.H. Lin, The effect of electrolytes on the aggregation kinetics of titanium dioxide nanoparticle aggregates, J. Nanoparticle Res. 14 (2012).
[24] G.C. Bushell, Y.D. Yan, D. Woodfield, J. Raper, R. Amal, On techniques for the measurement of the mass fractal dimension of aggregates, Adv. Colloid Interface Sci. 95 (2002) 1–50.
[25] K. Ishibashi, A. Fujishima, T. Watanabe, K. Hashimoto, Quantum yields of active oxidative species formed on TiO_2 photocatalyst, J. Photochem. Photobiol. A Chem. 134 (2000) 139–142.
[26] J.M. Herrmann, P. Pichat, Heterogeneous photocatalysis. Oxidation of halide ions by oxygen in ultraviolet irradiated aqueous suspension of titanium dioxide, J. Chem. Soc. Faraday Trans. 1 (76) (1980) 1138.
[27] M. Mehrvar, W.A. Anderson, M. Young, P.M. Reilly, Non-linear parameter estimation for a dynamic model in photocatalytic reaction engineering, Chem. Eng. Sci. 55 (2000) 4885–4891.
[28] E. Gerhard, Handbook of heterogeneous catalysis, Wiley-VCH, 2008.
[29] Y. Xu, C.H. Langford, Variation of Langmuir adsorption constant determined for TiO_2-photocatalyzed degradation of acetophenone under different light intensity, J. Photochem. Photobiol. A Chem. 133 (2000) 67–71.
[30] J.H. Esperson, Chemical kinetics and reaction mechanism, McGraw-Hill, 2002.
[31] M.R. Hoffmann, S.T. Martin, W. Choi, D.W. Bahnemannt, Environmental applications of semiconductor photocatalysis, Chem. Rev. 95 (1995) 69–96.
[32] L. Satuf, R.J. Brandi, A.E. Cassano, O.M. Alfano, Quantum efficiencies of 4-chlorophenol photocatalytic degradation and mineralization in a well-mixed slurry reactor, Ind. Eng. Chem. Res. 46 (2007) 43–51.
[33] A. Brucato, L. Rizzuti, Simplified modeling of radiant fields in heterogeneous photoreactors. 2. Limiting 'Two-Flux' model for the case of reflectance greater than zero, Ind. Eng. Chem. Res. 36 (1997) 4748–4755.
[34] M.L. Satuf, R.J. Brandi, A.E. Cassano, O.M. Alfano, Experimental method to evaluate the optical properties of aqueous titanium dioxide suspensions, Ind. Eng. Chem. Res. 44 (2005) 6643–6649.
[35] G. Li Puma, A. Brucato, Dimensionless analysis of slurry photocatalytic reactors using two-flux and six-flux radiation absorption-scattering models, Catal. Today. 122 (2007) 78–90.
[36] C. Turchi, Photocatalytic degradation of organic water contaminants: mechanisms involving hydroxyl radical attack, J. Catal. 122 (1990) 178–192.
[37] R.L. Pozzo, R.J. Brandi, A.E. Cassano, M.A. Baltanás, Photocatalytic oxidation of oxalic acid in dilute aqueous solution, in a fully illuminated fluidized bed reactor, Chem. Eng. Sci. 65 (2010) 1345–1353.
[38] M. Saran, K.H. Summer, Assaying for hydroxyl radicals: hydroxylated terephthalate is a superior fluorescence marker than hydroxylated benzoate, Free Radic. Res. 31 (1999) 429–436.
[39] A. Rincon, Effect of pH, inorganic ions, organic matter and H_2O_2 on *E. coli* K12 photocatalytic inactivation by TiO_2 implications in solar water disinfection, Appl. Catal. B Environ. 51 (2004) 283–302.
[40] A. Turolla, M. Fumagalli, M. Bestetti, M. Antonelli, Electrophotocatalytic decolorization of an azo dye on TiO_2 self-organized nanotubes in a laboratory scale reactor, Desalination 285 (2012) 377–382.
[41] D.M. Hamby, A review of techniques for parameter sensitivity analysis of environmental models, Environ. Monit. Assess. 32 (1994) 135–154.